Dear Guilia,

we have now implemented your suggestions (marked with blue color on the attached pages, revised figures 2, 4, and 6 not explicitly marked).

Considering DEMs of higher resolution would indeed be interesting. I would hope that the role of the parameter b will become clearer then. So far there is still some kind of interference between θ and b in the way that a decrease in θ might be almost compensated by an increase in b. As a consequence, my preliminary comparison of the b values of different catchments is not really unique. As the parameter b quantifies the relative contribution of non-fluvial processes to total erosion, I would hope that it could finally be related to rock or soil properties or to precipitation. Maybe a higher resolution could really help there, although I suspect that the overall results will not change much.

All the best,

Stefan

Stefan Hergarten

Albert-Ludwigs-Universität Freiburg

Institut für Geo- und Umweltnaturwissenschaften

Abteilung Geologie

Prof. Dr. Stefan Hergarten
Vertretungsprofessor für
Oberflächennahe Geophysik

Albertstraße 23 b
79085 Freiburg

Tel. 0761/203-6471
Fax 0761/203-6496

stefan.hergarten@geologie.uni-freiburg.de
www.hergarten.at

Freiburg, 11. 12. 2015

as the erosion rate in principle depends on the discharge instead of the catchment size.

Physically based models of bedrock incision suggest that the concavity index θ of a steady-state bedrock river under homogeneous conditions does not only depend on the constitutive laws of the erosion process, but also on the cross-sectional geometry of the channels (e.g., Whipple, 2004; Whipple et al., 2013; Lague, 2014). This explains some variation in θ around the value $\theta \approx 0.5$ originally found by Hack (1957) or around the reference value $\theta_{\text{ref}} = 0.45$ being widely assumed for perfect bedrock channels under homogenous steady-state conditions (Whipple et al., 2013; Lague, 2014).

A range of θ between about 0.4 and 0.7 has been found under relatively homogeneous conditions (e.g., Whipple, 2004; Whipple et al., 2013), while a wider range from less than 0.2 in steep headwater channels to more than 1 in some alluvial channels has been reported (Brummer and Montgomery, 2003; Montgomery, 2001; Sofia et al., 2015). Apparent variations in θ may also arise from spatial inhomogeneity or non-steady topography. Analyzing channel slopes at constant catchment sizes, Hergarten et al. (2010) found a strong positive correlation between surface elevation and slope in several orogens, suggesting a correlation between uplift rate and elevation. This correlation will lead to a higher apparent steepness index when following individual rivers, which may explain why the majority of the values of θ found in nature are greater than $\theta_{\text{ref}} = 0.45$.

Compared to the concavity index θ, less is known about the exponent n as it cannot be determined from individual equilibrium river profiles under uniform conditions. According to Eq. (4), the exponent n can be determined by comparing river segments being in equilibrium with different uplift rates, and the results tentatively suggest that n should not be far away from one (Wobus et al., 2006).

Using Eq. (2), the evolution of the surface elevation $H(x,t)$ along the stream profile through time under a given uplift rate U follows the partial differential equation

$$\frac{\partial H}{\partial t} = U - K\left(\left(\frac{A}{A_0}\right)^{\theta}\frac{\partial H}{\partial x}\right)^{n} \tag{3}$$

where the linear coordinate x follows the upstream direction of the considered river. Both U and K may vary spatially and temporally.

The simplest interpretation of Eq. (3) refers to steady-state topography where uplift and erosion are in local equilibrium. Under these conditions, the ratio of uplift rate and erodibility can be directly obtained from the steepness index (Eq. 1) according to

$$\frac{U}{K} = \left(\frac{k_s}{A_0^{\theta}}\right)^{n}. \tag{4}$$

The most interesting applications of the stream-power erosion equation (Eq. 3), however, concern nonequilibrium river profiles due to temporally changing uplift rates or due to climate-induced changes in the erodibility. If such changes are discontinuous, they result in distinct knickpoints propagating in upstream direction.

2 The χ transformation and its limitation

Recently, the so-called χ plot (or χ transformation) introduced the perhaps most important methodic progress in evaluating and interpreting longitudinal river profiles since the seminal work of Howard (1994). It transforms the upstream coordinate x to a new coordinate χ in such a way that the inherent curvature of equilibrium profiles due to the reduction of catchment size in upstream direction vanishes. The catchment size A can be eliminated from Eq. (3) if the transformation satisfies the condition

$$\frac{dx}{d\chi} = \left(\frac{A}{A_0}\right)^{\theta}, \tag{5}$$

which can be achieved by

$$\chi(x) = \int_{x_0}^{x} \left(\frac{A(\xi)}{A_0}\right)^{-\theta} d\xi \tag{6}$$

where x_0 is an arbitrary reference point. As the channel slope is $S = \frac{\partial H}{\partial x}$, the erosion rate (Eq. 2) can be written in the form

$$E = K\left(\frac{dx}{d\chi}\frac{\partial H}{\partial x}\right)^{n} \tag{7}$$

$$= K\left(\frac{\partial H}{\partial \chi}\right)^{n}. \tag{8}$$

thus, the local erosion rates is directly related to the slope of the river profile in the H vs. χ representation, and Eq. (3) simplifies to

$$\frac{\partial H}{\partial t} = U - K\left(\frac{\partial H}{\partial \chi}\right)^{n}. \tag{9}$$

The solutions of this equation and their potential for unraveling the uplift and erosion history have been discussed by Royden and Perron (2013), and a formal inversion procedure for the linear case ($n = 1$) has been presented by Goren et al. (2014).

The most striking property of the χ transformation is immediately recognized in Eq. (9): If U and K are spatially homogeneous, all upstream paths starting from x_0 are described by the same differential equation, so that the H vs. χ curves of all tributaries must collapse with the H vs. χ curve of the main stream. Conversely, spatial inhomogeneity results in a deviation of the curves belonging to different branches that increases in upstream direction. Thus, a narrow bunch of H vs. χ curves with a nonlinear overall shape is the fingerprint of temporal variations under spatially homogeneous

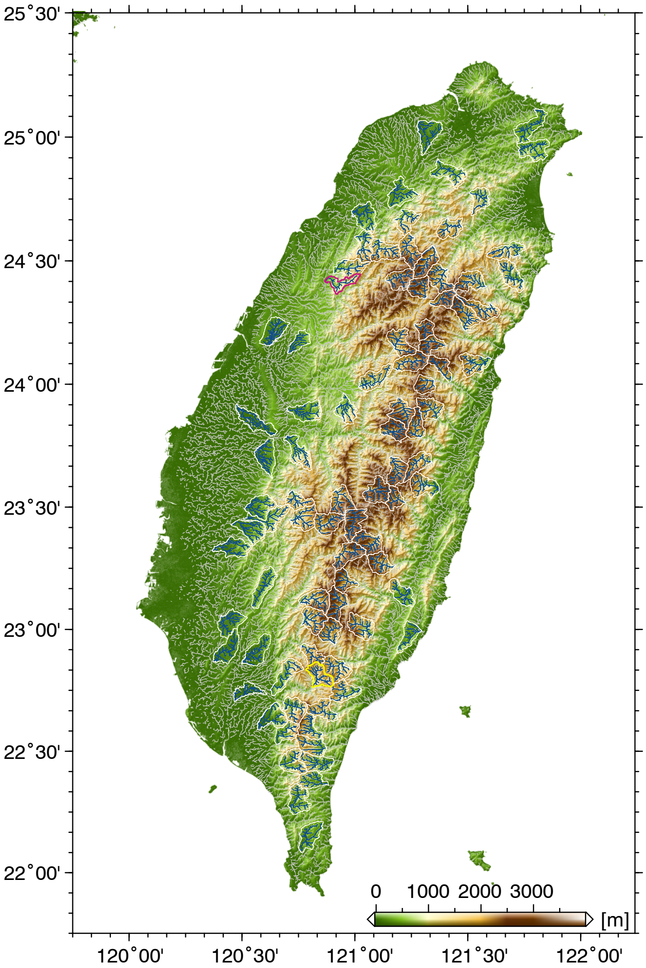

Figure 2. Map of the 89 considered catchments in Taiwan with catchment sizes $A \approx 100\,\mathrm{km}^2$. The two catchments bordered in magenta and yellow are considered in detail in Figs. 4–6.

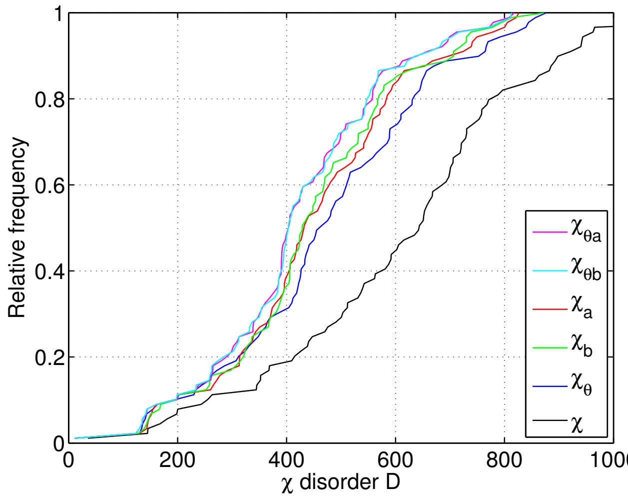

Figure 3. Cumulative distribution of the χ disorder for the 89 considered catchments in Taiwan for $0.01\,\mathrm{km}^2 \leq A \leq 100\,\mathrm{km}^2$. Each curve describes the relative number of the catchments with a χ disorder lower than or equal to the value D on the x axis.

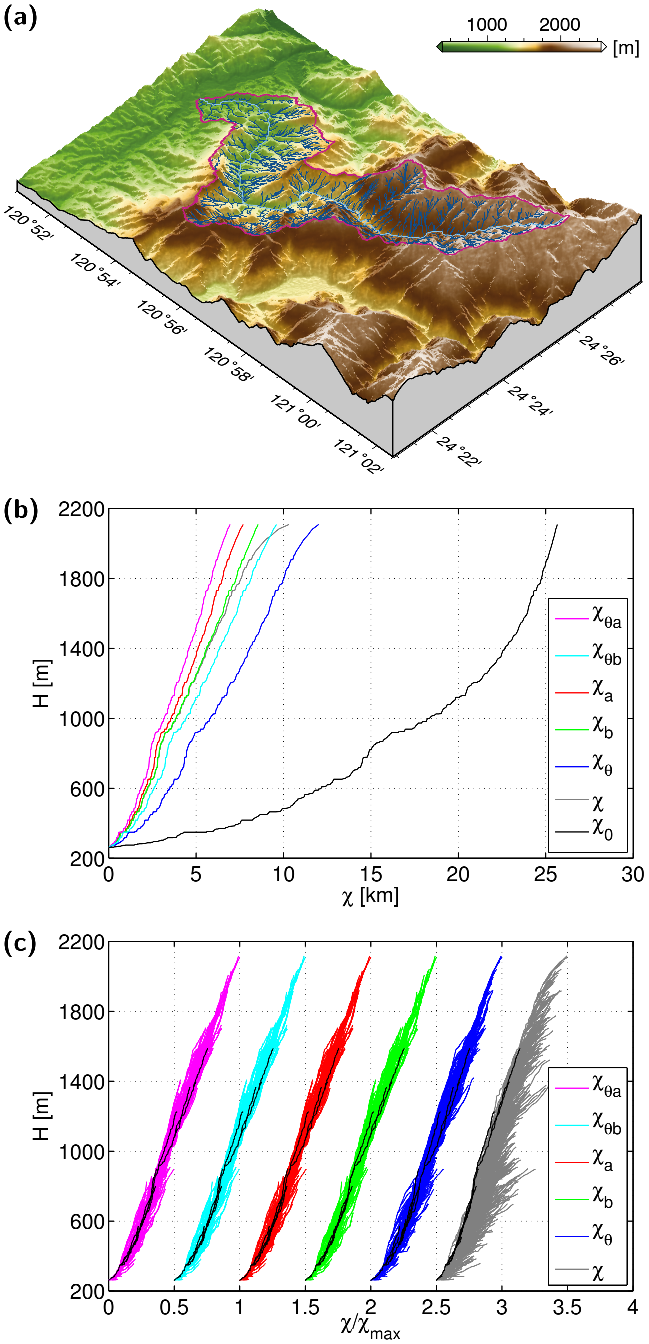

Figure 4. The mountainous catchment in Taiwan with the lowest χ disorder. (a) Topography and drainage pattern for $A \geq 0.01$ km^2. The largest river is drawn in light blue. (b) H vs. χ plots of the main river. χ_0 refers to $\theta = 0$, so that $\chi_0 = x$, and the plot describes the original river profile. (c) H vs. χ plots for the entire drainage network. The plots are shifted horizontally in order to avoid overlapping curves. The black lines show the part of the drainage network with $A \geq 1$ km^2.

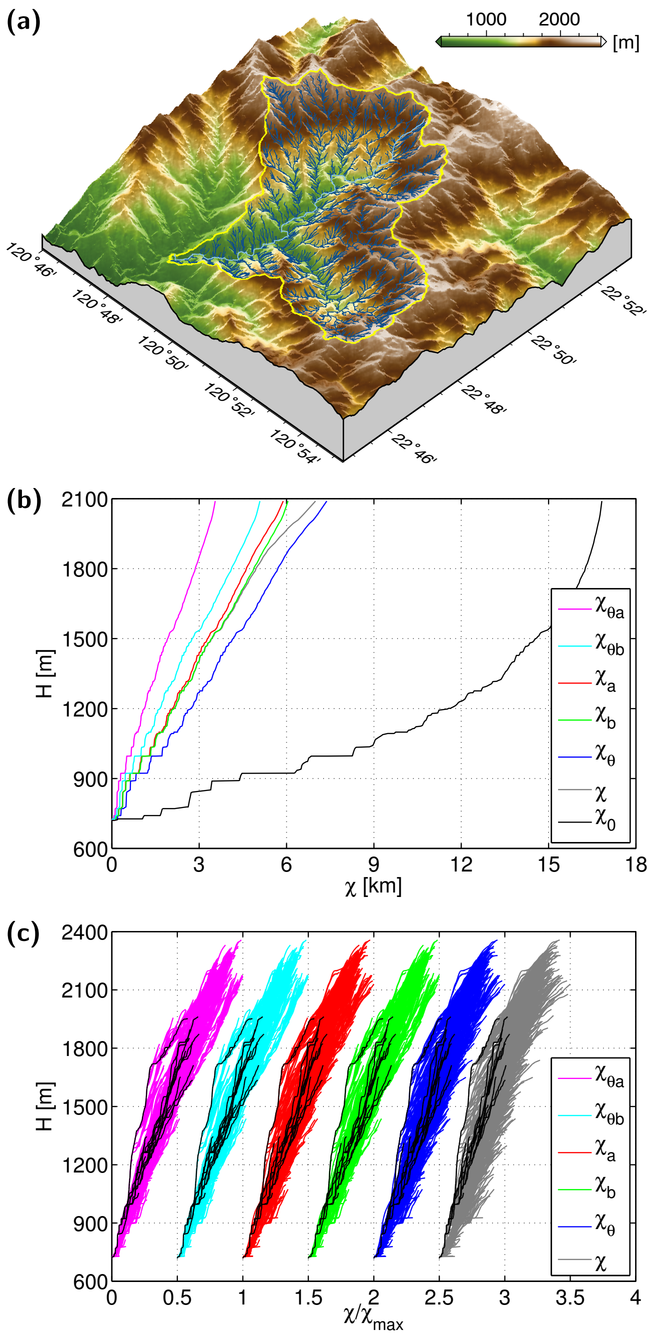

Figure 5. A catchment in Taiwan with a rather high χ disorder. (a) Topography and drainage pattern for $A \geq 0.01$ km^2. The largest river is drawn in light blue. (b) H vs. χ plots of the main river. χ_0 refers to $\theta = 0$, so that $\chi_0 = x$, and the plot describes the original river profile. (c) H vs. χ plots for the entire drainage network. The plots are shifted horizontally in order to avoid overlapping curves. The black lines show the part of the drainage network with $A \geq 1$ km^2.